AGU PUBLICATIONS

Geophysical Research Letters

RESEARCH LETTER
10.1002/2015GL066768

Key Points:
- Contrasting ENSO amplitude changes occur in CMIP5 models due to abrupt CO_2 quadrupling
- The difference in the central tropical Pacific ZWS forcing efficiency causes the contrasting amplitude changes
- The ENSO amplitude changes are linked with changes in zonal wind-convection coupling in the central tropical Pacific

Supporting Information:
- Supporting Information S1

Correspondence to:
H. A. Rashid,
harun.rashid@csiro.au

Citation:
Rashid, H. A., A. C. Hirst, and S. J. Marsland (2016), An atmospheric mechanism for ENSO amplitude changes under an abrupt quadrupling of CO_2 concentration in CMIP5 models, *Geophys. Res. Lett.*, *43*, 1687–1694, doi:10.1002/2015GL066768.

Received 28 OCT 2015
Accepted 29 JAN 2016
Accepted article online 3 FEB 2016
Published online 24 FEB 2016

An atmospheric mechanism for ENSO amplitude changes under an abrupt quadrupling of CO_2 concentration in CMIP5 models

Harun A. Rashid[1], Anthony C. Hirst[1], and Simon J. Marsland[1]

[1]CSIRO Oceans and Atmosphere, Aspendale, Australia

Abstract We investigate the impact of a quadrupled CO_2 concentration on the simulated El Niño–Southern Oscillation (ENSO) amplitudes in 19 Coupled Model Intercomparison Project phase 5 (CMIP5) climate models. The amplitude of ENSO-related sea surface temperature (SST) variability decreases in 11 of these models, and increases in the rest, in response to the enhanced radiative forcing. These opposing amplitude changes are predominantly explained by opposite changes in the time-lagged SST response to a given central Pacific zonal wind stress (ZWS) forcing, with the net heat flux forcing and the SST-ZWS feedback playing smaller roles. We find a robust relationship between the changes in the ZWS forcing efficiency and those in the ZWS-deep convection coupling in the central-western Pacific, indicating an important role for this coupling in ENSO amplitude changes. Indeed, the projected change in this coupling is indicative of the projected change in ENSO-related SST variability.

1. Introduction

El Niño–Southern Oscillation (ENSO) is the dominant mode of interannual variability that originates in the tropical Pacific but influences the regional weather and climate variability all over the world [*Trenberth et al.*, 1998]. Any future changes in the regional weather and climate variability, due to the projected increases in anthropogenic greenhouse gas (GHG) emissions, will likely be modulated by possible changes in the ENSO properties. However, a reliable projection of the future changes in ENSO properties has remained a great scientific challenge, despite many past investigations on this subject using coupled general circulation models (CGCMs) [*Merryfield*, 2006; *Philip and van Oldenborgh*, 2006; *Stevenson*, 2012; *Power et al.*, 2013; *Cai et al.*, 2014, 2015; *Kim et al.*, 2014b; *Chen et al.*, 2015]. Part of the problem is diversity of model results. While more recent work has uncovered robust projected changes in ENSO-driven precipitation variability [e.g., *Power et al.*, 2013; *Chung et al.*, 2014], a high degree of uncertainty in underlying changes in ENSO-related sea surface temperature (SST) variability remains in the latest generation of climate models. There is a broader agreement among the models regarding the changes in the mean state, with most of the models projecting a warmer tropical Pacific, a reduced east-west SST gradient, and a weaker Walker circulation [e.g., *Philip and van Oldenborgh*, 2006; *Vecchi and Soden*, 2007]. Therefore, the uncertainty in the projected ENSO-related SST variability appears to primarily stem from the differences among models in representing the ENSO forcings and feedbacks [e.g., *Collins et al.*, 2010], although the differences in the simulated mean state may also contribute [*Yeh et al.*, 2010; *DiNezio et al.*, 2012].

Recent studies have focused on the simulated ENSO forcings and feedbacks in order to understand the causes of uncertainty in ENSO-related SST variability in CGCMs. Some of the main ENSO processes may be described conceptually as [e.g., *van Oldenborgh et al.*, 2005] follows: the central equatorial Pacific zonal wind stress (ZWS) anomalies force the zonal current anomalies and the thermocline anomalies, which then affect the SST anomalies in the central eastern Pacific and the eastern Pacific, respectively, through the zonal advection and the subsurface ocean dynamics. The SST anomalies in turn feedback on the central Pacific ZWS anomalies, thus completing the so-called Bjerknes feedback loop. The Ekman feedback also contributes positively to the ENSO growth. *Philip and van Oldenborgh* [2006] examined the various components of the Bjerknes feedback loop in five Coupled Model Intercomparison Project phase 3 (CMIP3) models and found that the changes in ENSO amplitude contributed by these components largely cancel each other, resulting in no statistically significant ENSO change under global warming. Other investigators also studied, mostly from an oceanic perspective, aspects of the feedback loop, revealing the importance of the zonal advection and thermocline feedbacks, and also of changes in the upper ocean structure, in ENSO amplitude changes [*Merryfield*, 2006; *Yeh et al.*, 2010; *DiNezio et al.*, 2012; *Kim et al.*, 2014b; *Linz et al.*, 2014; *Chen et al.*, 2015].

Here we investigate the causes of changes in the ENSO-related SST variability (hereafter, ENSO amplitude) under global warming, focusing on the atmospheric forcings and feedbacks. The most important contributions to the ENSO's overall growth rate, as measured by the BJ index [*Jin et al.*, 2006], come from the thermal damping and the thermocline feedback and to a lesser extent the zonal advective feedback [*Lübbecke and McPhaden*, 2013; *Kim et al.*, 2014a]. The two latter feedbacks are positive ENSO feedbacks that are dynamically linked to each other and are in phase [*Jin and An*, 1999; *An and Jin*, 2001]. Additionally, these feedbacks are mainly controlled by the ocean dynamic responses to the ZWS forcing [*Kim et al.,* 2014a, Figure 4]. It follows that the equatorial Pacific ZWS forcing of SST (to be distinguished from the ZWS feedback) encapsulates both these oceanic feedbacks and is therefore an effective diagnostic tool for understanding the changes in ENSO dynamics. Here we examine the effect of changes in this important ENSO forcing, as well as in the ZWS and net heat flux (NHF) feedbacks, on ENSO amplitude changes under global warming.

We find opposing changes in the projected ENSO amplitude in two groups of CMIP5 models, which are highly correlated with the corresponding changes in the ZWS forcing efficiency (hereafter, ZFE). (The ZFE here refers to the time-lagged changes in eastern Pacific SSTs forced by a unit change in the central equatorial Pacific ZWS anomalies.) The changes in ZFE, in turn, are strongly correlated with changes in the central Pacific deep convection. The strength of this surface zonal wind-deep convection coupling is found to be a good indicator of whether a particular model will simulate a strengthening or weakening ENSO under the abruptly quadrupled CO_2 (hereafter, a4xCO_2) concentration.

2. Model Data and Analysis Methods

We analyze data from 19 pairs of the piControl and abrupt4xCO_2 experiments from the CMIP5 archive [*Taylor et al.*, 2012]. These two experiments differ only in that the CO_2 concentration specified in the abrupt4xCO_2 experiment (from the beginning) is 4 times that in the piControl experiment. The models were chosen solely based on the availability of variables (described below) from both experiments required for the present analysis. The standard simulation length of the abrupt4xCO_2 experiment is 150 years; we discard data for the first 30 years (when rapid adjustments occur in the abrupt4xCO_2 experiment) and use the next 120 years of data from both the experiments. However, we have repeated the calculations also using the last 100 years and the full 150 years of data, with essentially the same conclusions as those obtained from the last 120 years. The variables analyzed are SST, ZWS, precipitation, and the net heat flux (computed from its components: shortwave flux, longwave flux, latent heat flux, and sensible heat flux). The variables from different models were first interpolated to a common grid (1.25° latitude × 1.875° longitude). We then detrended the data by subtracting a quadratic fit to the variables, to remove any trend resulting from slow adjustments to the CO_2 forcing in the abrupt4xCO_2 experiment or from small model drifts in the piControl experiment. The anomalies were computed by removing the climatological annual cycle from the detrended data; these anomalies were used to calculate all the statistics, except for the time means, shown in the figures.

The ENSO pattern and time series are defined by the leading empirical orthogonal function (EOF) and principal component (PC) of SST anomalies over the equatorial Pacific (10°S – 10°N, 120°E – 80°W). The standard deviations of the PC time series from different models are used to measure their ENSO amplitudes. The qualitative nature of the results presented below does not change if the Niño-3 index (the SST anomalies averaged over the Niño-3 region; 5°S–5°N, 150°W–90°W) is used in place of PC1 (Table S1 in the supporting information). The other diagnostics used in this study (e.g., ZFE and the zonal wind-deep convection coupling) are defined at appropriate places. The changes in various quantities due to the a4xCO_2 concentration are quantified by the ratios of those quantities computed from the abrupt4xCO_2 and piControl experiments; these two keywords are used interchangeably in this paper. The results remain qualitatively unchanged if an alternative measure for the changes, namely, the difference between the abrupt4xCO_2 and piControl experiments is used instead.

3. ENSO Amplitude Changes

The changes in ENSO amplitude between the piControl and the abrupt4xCO_2 simulations for the CMIP5 models, and the statistical significance of the changes, are shown in Figure 1. Out of the 19 models, 8 models show a strengthening of ENSO (orange bars), and 11 models show a weakening (blue bars) (Figure 1a). The spatial structure of ENSO, as represented by the leading SST EOF over the tropical Pacific, does not change

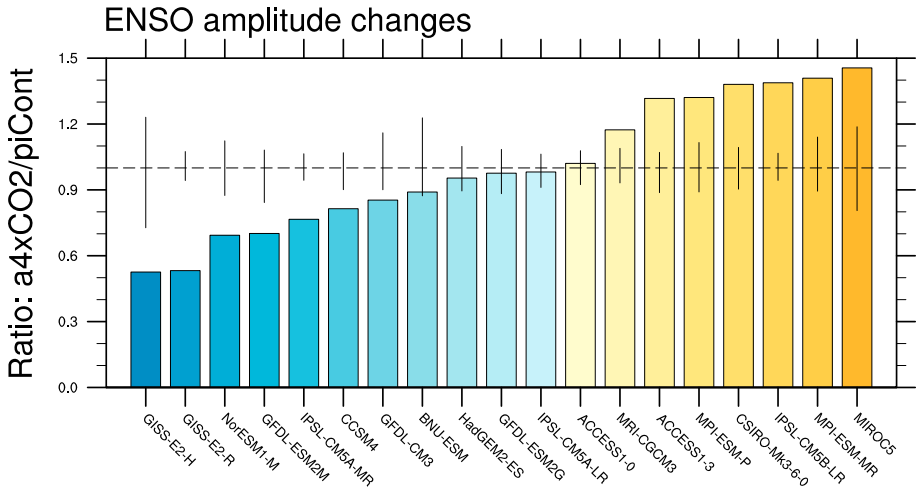

Figure 1. ENSO amplitude changes under global warming and their statistical significance. Ratios (abrupt4xCO_2 to piControl) of ENSO amplitudes for 19 coupled models from the CMIP5 archive are shown. The blue (orange) bars, with ratios less (greater) than 1, represent the models for which the ENSO amplitude decreases (increases) in the abrupt4xCO_2 simulation with respect to the corresponding piControl simulation. The thin vertical lines indicate the 99% confidence limits for the changes in ENSO amplitude resulting from the natural variability, estimated from the 500 year piControl experiments.

significantly from the piControl to the abrupt4xCO_2 simulation (Figures S1a and S1b). This is consistent with the findings of *Power et al.* [2013] who examined changes in CMIP5 and CMIP3 models under four different greenhouse gas emissions scenarios for the 21st century. This indicates that our results may have applicability beyond the idealized abrupt changes to GHG concentration considered in this study.

The thin vertical lines in Figure 1 show the 99% confidence limits for the changes in ENSO amplitude resulting from the natural variability alone, estimated from the 500 year piControl experiments. For each model, the standard deviations of PC1 over a 120 year sliding window were first calculated, then the ratios of all the standard deviations to the median standard deviation (taken to represent the "true" value for the piControl experiment) were calculated. The 0.5th and 99.5th percentiles of these ratios then constitute the 99% confidence limits (a two-sided test). The ratios of ENSO amplitude falling outside these limits may be considered as statistically significant. A second measure of the statistical significance for the ENSO amplitude changes, estimated using the *F* test, also shows consistent results: the largest ENSO amplitude changes are also statistically significant (Figure S2). Some recent studies suggested that the multimodel mean change in ENSO amplitude due to global warming is statistically indistinguishable from zero [e.g., *Stevenson*, 2012]. Our result is not inconsistent with this, with about equal numbers of models showing statistically significant opposite changes in the ENSO amplitude (implying that the multimodel mean change would be very small).

While the opposing ENSO amplitude changes under global warming have been discussed in previous multimodel studies, the reason for such discrepancy among models has not been well understood [*Philip and van Oldenborgh*, 2006; *Collins et al.*, 2010], although some suggestions have been made focusing on the oceanic processes [e.g., *Yeh et al.*, 2010; *DiNezio et al.*, 2012]. Next, we seek to explain this discrepancy among the CMIP5 models in terms of differences in their simulated atmospheric forcing and feedbacks of the ENSO-related SST variability.

4. Association With ENSO Forcings

The associations between the changes in ENSO amplitude and the changes in the ZFE (Figure 2a) and the NHF forcing efficiency (NFE) (Figure 2b) are demonstrated in Figure 2. The ZFE was estimated by regressing the Niño-3 SST index onto the ZWS anomalies averaged over the Niño-4 region (5°S–5°N, 160°E–150°W; hereafter, the Niño-4 ZWS index). The regression coefficients were computed with the ZWS index leading the SST index by 2 months, to allow for a nonzero time lag between the wind stress forcing and the SST response. This is motivated by observations, where the regression between the ZWS and SST indices is a maximum when the former leads by 2 months; for CMIP5 models, the lead time varies from 0 to 3 months (Figures S3a and S3b).

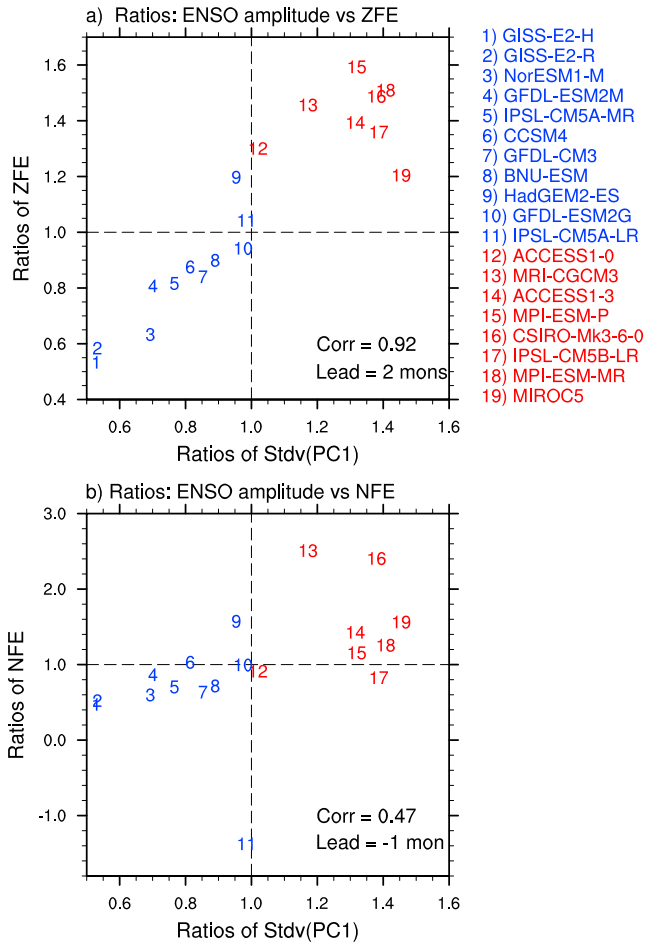

Figure 2. Scatter diagrams of ENSO amplitude changes versus the changes in the dominant atmospheric forcings of ENSO due to the abrupt quadrupling of the CO_2 concentration. (a) The ratios (abrupt4xCO_2 to piControl) of the zonal wind stress forcing efficiency (ZFE) and (b) the ratios of the net heat flux forcing efficiency (NFE) are plotted against the ratios of ENSO amplitudes. The numbers with blue (orange) color indicate the models for which the ENSO amplitude decreases (increases) in the abrupt4xCO_2 simulation with respect to the piControl simulation. The linear correlation coefficient between the quantities plotted along the *x* and *y* axes is shown in the respective plot. The "lead" refers to the months by which the zonal wind stress, and net heat flux indices lead the Niño-3 index in the calculation of the regression coefficients. The critical value of the linear correlation coefficient at 95% significance level ($p = 0.05$) is 0.456 for df = N–2 = 17. Note that the individual NFEs are negative; hence, their ratios are positive (except for model number 11).

The scatter plot in Figure 2a shows a strong positive correlation ($r = 0.92$) between the changes in ENSO amplitude and those in the ZFE for different models. That is, the models simulating a stronger (weaker) ENSO under the a4xCO_2 concentration are those that simulate a stronger (weaker) SST response to a given central Pacific ZWS anomaly, except for two models (number 9 and 11) showing very small ENSO amplitude changes (Figure 1). The correlation is the strongest when the ZWS index leads the SST index by a few months; this is consistent with the view that the role of the ZWS anomalies is a dominant one in the coupled ZWS-SST interactions in the tropical Pacific [*Clarke*, 2014]. These time-lagged interactions may be understood as the central equatorial Pacific ZWS anomalies influencing the remote eastern Pacific SSTs through the zonal advection and the subsurface ocean dynamics, as discussed in section 1. While the feedback of the SST anomalies on the ZWS anomalies is also significant, the changes in this ZWS feedback (defined as the contemporaneous regression of the Niño-4 ZWS index onto the Niño-3 SST index) do not have as strong correlation with the changes in ENSO amplitude as the changes in the ZFE have. A plot similar to Figure 2a, but replacing the ratios of ZFEs by the ratios of ZWS feedbacks, clearly shows this smaller correlation ($r = 0.51$, Figure S4a).

Figure 2b shows a similar plot for the changes in ENSO amplitude versus the changes in the NFE, the latter being defined as the regression coefficient of the Niño-3 SST index onto the Niño-3 averaged NHF anomalies. The regression, which in this case is negative, is a minimum when the NHF anomalies lag SST anomalies by 0 to 1 month in the observation and CMIP5 models (Figures S3a and S3b); therefore, we have chosen a lead time of −1 month in Figure 2b. As for the ZFE, there is a positive correlation (albeit smaller) between the changes in the NFE and the ENSO amplitude changes. There is also a positive correlation, of similar magnitude, between the changes in the NHF feedback and the ENSO amplitude changes (Figure S4b). The positive correlation for both cases indicates that the NHF anomalies merely respond to the SST anomalies, i.e., the larger the SST anomalies, the larger the associated NHF damping is and vice versa. In other words, the NHF damps the SST anomalies [e.g., *Zebiak and Cane*, 1987; *Philip and van Oldenborgh*, 2006] to balance the other forcings, including that from the ZWS anomalies.

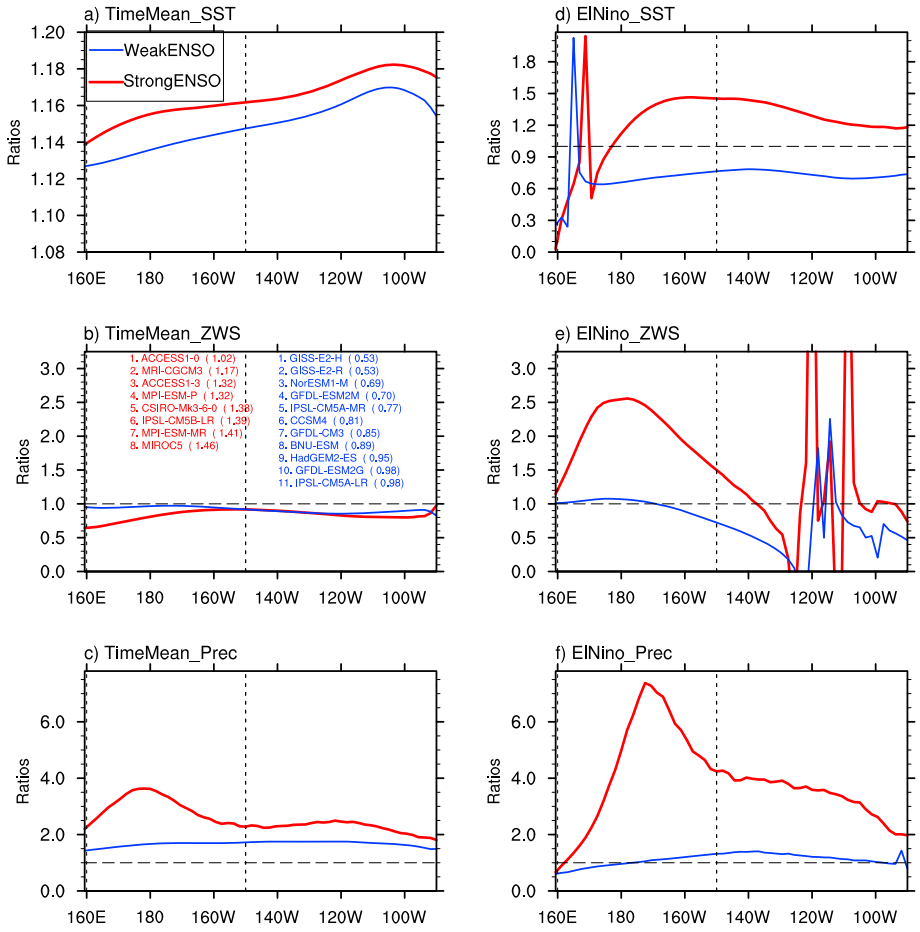

Figure 3. Ensemble means of the ratios of statistics of (a and d) SST, (b and e) zonal wind stress, and (c and f) precipitation for the two groups of models showing increasing (red curve) and decreasing (blue curve) ENSO amplitudes under the global warming. The ratios are shown, as a function of longitude, for two statistics: time means (left-hand side column) and the El Niño composites (right-hand side column). The ratios (abrupt4xCO_2 to piControl) were first calculated for individual models and then ensemble averaged separately for the two groups of models. The El Niño composites were constructed by first smoothing the PC1 time series with a 5 month running average and then averaging the variable of interest over the months for which the smoothed PC1 exceeded a 1 standard deviation threshold value. The variables were averaged over latitudes (5°S – 5°N) before computing the statistics.

The above analysis reveals the dominant contribution of the changes in ZFE to ENSO amplitude changes under the a4xCO_2 concentration. It is therefore of interest to understand the mechanism behind the simulation of stronger ZFEs in a subset of the models (with stronger ENSOs) but weaker ZFEs in the rest of the models (with weaker ENSOs).

5. Mechanism of ENSO Amplitude Changes

The surface zonal wind, and hence the ZWS, in the tropical Pacific is closely tied to the deep tropical convection that is most active in the western Pacific under normal conditions [*Gill*, 1980; *Clarke*, 1994; *Chiang et al.*, 2001]. It is well known that the tropical convection shifts eastward to the central Pacific during El Niño events when the central and eastern tropical Pacific anomalously warms. Under the global warming scenarios, climate models also simulate a tropical warming of several degree Celsius [e.g., *DiNezio et al.*, 2009; *Collins et al.*, 2010]. The combined effect of El Niño and enhanced CO_2-induced warmings in the Pacific brings about a significant shift in the tropical convection [*Power et al.*, 2013; *Chung et al.*, 2014], suggesting a considerable change also in the simulated ZWS.

Figure 3 shows the ensemble mean of ratios (abrupt4xCO_2 to piControl) for the time mean and anomalous SST, ZWS, and rainfall over the equatorial Pacific. The time mean SST increases under global warming in both

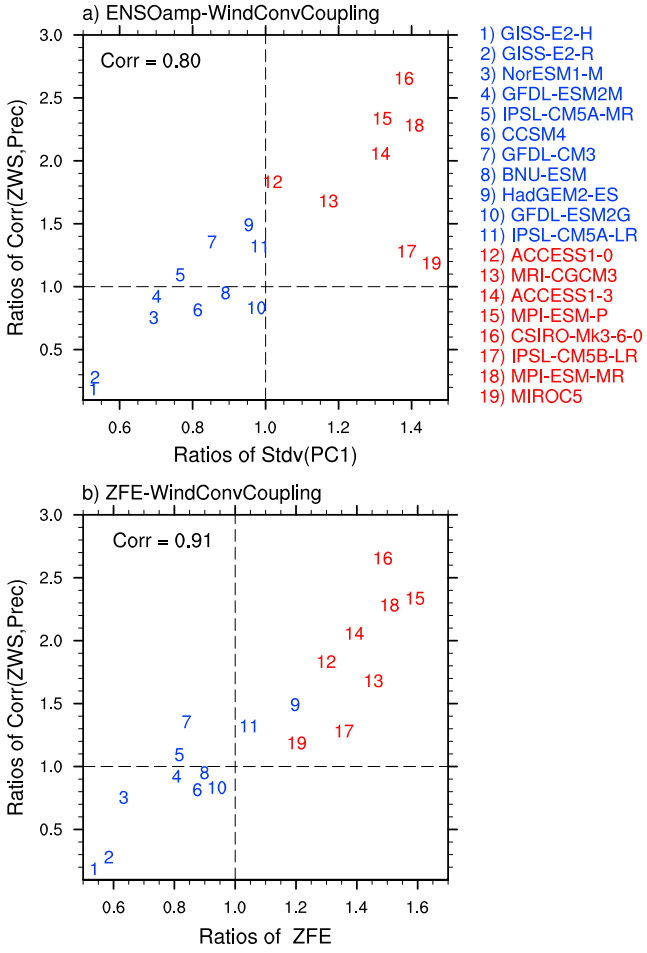

Figure 4. Scatter diagrams of changes in the zonal wind stress-deep convection coupling versus the changes in (a) ENSO amplitude and (b) ZFE, due to the abrupt quadrupling of the CO_2 concentration. Other relevant information is provided in the caption of Figure 2.

groups of models, with the "stronger ENSO" group showing a slightly larger increase than the "weaker ENSO" group throughout the equatorial Pacific (Figure 3a). The largest mean SST changes occur in the eastern Pacific, which reduces the equatorial SST gradient. Consistent with this, the time mean easterly ZWS weakens for both group of models, but the group with strengthening ENSOs simulate a larger weakening in the western Pacific (Figure 3b). The time mean rainfall also increases in both groups of models, but the largest increase occurs for the group of models with strengthening ENSOs, again in the western Pacific (Figure 3c).

The ensemble mean ratios of the composite El Niño anomalies show an increase and decrease of SST responses in the groups of models with strengthening and weakening ENSOs, respectively (by definition; Figure 3d). For the ZWS anomalies (Figure 3e), the models with strengthening ENSOs show substantially stronger westerly anomalies in the central-western Pacific (the Niño-4 region) with the maximum centred on the date line, whereas the models with weakening ENSOs show slightly weaker westerly anomalies in the eastern part of this region. The changes in rainfall response show a strong increase for the group of models with strengthening ENSOs, with the maximum increase occurring to the slightly east of the date line (Figure 3f). In this group of models, the maximum change in rainfall response occurs just to the east of the location of the strongest westerly ZWS response, suggesting a stronger coupling between the surface westerlies and the deep convection in the tropical central Pacific under global warming. On the other hand, the changes in rainfall response in the group of models with weakening ENSOs are very small, and the (weak) maximum change is located in the eastern Pacific. Thus, there are no significant changes in the coupling between the surface westerlies and the deep convection in this group of models.

The link between the ENSO amplitude changes and the changes in the surface zonal wind-deep convection coupling is clearly demonstrated in Figure 4, which shows the changes in the ZWS-precipitation coupling against the changes in ENSO amplitude (Figure 4a) and in ZFE (Figure 4b). The ZWS-precipitation coupling was defined as the longitude average over the Niño-4 region of the linear correlations between the ZWS anomalies and the precipitation anomalies at different longitudes. The coupling is strengthened (weakened) under the a4xCO_2 concentration in the group of models with strengthening (weakening) ENSOs (Figure 4a). There is a strong positive correlation between these two changes ($r = 0.80$), with all (most) of the models with a strengthening (weakening) ENSO also showing a strengthening (weakening) of this coupling. The association is even stronger between the changes in the ZWS-precipitation coupling and the changes in the ZFE ($r = 0.91$; Figure 4b). Therefore, a main cause for the two groups of models showing opposing ENSO responses to global warming appears to be the opposing changes in the strength of coupling between the deep convection and the surface zonal winds in the central Pacific.

6. Conclusions

We have investigated the impact of the a4xCO_2 concentration on the simulation of ENSO amplitudes in 19 CMIP5 models (chosen based on the data availability). Fourteen of these models show statistically significant ENSO amplitude changes in response to the a4xCO_2 concentration, with one half of them showing a strengthening of ENSO and the other half showing a weakening. We find that these differing responses are closely related to the opposite changes in the eastern equatorial Pacific SST response to the central-western Pacific ZWS anomalies and in the ZWS-precipitation coupling in the two groups of models. Specifically, we find that

1. Global warming-induced changes in ENSO-related SST variability in the eastern equatorial Pacific are highly correlated with the changes in SST response to a given antecedent ZWS anomaly (i.e., the ZFE) in the central equatorial Pacific. That is, the models simulating stronger (weaker) ENSO events under global warming also simulate stronger (weaker) ZFEs.
2. The stronger ZFEs, in the subset of the models simulating strengthening El Niño events, are accompanied by the occurrence of stronger deep convections in the central equatorial Pacific (as indicated by higher precipitation rates). The ZWS and precipitation anomalies are also highly correlated in these models, indicating that the surface zonal wind-deep convection coupling strengthens in the central Pacific under global warming in this group of models.
3. In contrast, in the group of models that simulate weakening ZFEs and weakening ENSOs, the El Niño-associated deep convections remain essentially unchanged under global warming, leading to a weaker surface zonal wind-deep convection coupling.
4. The opposite ENSO responses to the a4xCO_2 concentration in two groups of models occur despite the simulated mean SST and precipitation increase in all models.

These results suggest an important role for the surface zonal wind-deep convection coupling in determining the nature of ENSO amplitude change in response to the a4xCO_2 concentration. A positive feedback loop, incorporating the coupling between atmospheric convection, low-level westerlies, and SST anomalies in the warm-pool region, was proposed to explain the evolution of the 1982–1983 El Niño event [*Gill and Rasmusson*, 1983]. The present study highlights the importance of a similar feedback loop in determining the ENSO response to global warming and complements the previous studies describing the role of the oceanic processes. It will be interesting to explore in a future study the reason for the opposing changes in the surface zonal wind-deep convection coupling strength due to global warming in the two groups of CMIP5 models, which we have not addressed here. Such an investigation will involve a detailed examination of the dynamical and thermodynamical processes influencing deep convection in the central-western Pacific.

Acknowledgments

We thank the three official reviewers for their insightful comments, which helped clarify the presentation of the result. Thanks are also due to Jaclyn Brown and Scott Power for their valuable comments on an earlier draft of this paper, which helped improve the paper. This work has been undertaken as part of the Australian Climate Change Science Program, funded jointly by the Australian Government Department of the Environment, the Bureau of Meteorology, and CSIRO. We acknowledge the World Climate Research Programme's Working Group on Coupled Modelling, which is responsible for CMIP, and we thank the climate modeling groups for producing and making available their model output. For CMIP the U.S. Department of Energy's Program for Climate Model Diagnosis and Intercomparison provides coordinating support and led development of software infrastructure in partnership with the Global Organization for Earth System Science Portals. The CMIP5 model output used in this study may be downloaded freely from http://pcmdi9.llnl.gov/esgf-web-fe/ upon registration.

References

An, S. I., and F. F. Jin (2001), Collective role of thermocline and zonal advective feedbacks in the ENSO mode, *J. Clim.*, *14*(16), 3421–3432, doi:10.1175/1520-0442(2001)014<3421:CROTAZ>2.0.CO;2.

Cai, W., et al. (2014), Increasing frequency of extreme El Niño events due to greenhouse warming, *Nat. Clim. Change*, *5*(1), 1–6, doi:10.1038/nclimate2100.

Cai, W., et al. (2015), ENSO and greenhouse warming, *Nat. Clim. Change*, doi:10.1038/nclimate2743.

Chen, L., T. Li, and Y. Yu (2015), Causes of strengthening and weakening of ENSO amplitude under global warming in four CMIP5 models, *J. Clim.*, *28*, 3250–3274, doi:10.1175/JCLI-D-14-00439.1.

Chiang, J. C. H., S. E. Zebiak, and M. A. Cane (2001), Relative roles of elevated heating and surface temperature gradients in driving anomalous surface winds over tropical oceans, *J. Atmos. Sci.*, *58*, 1371–1394.

Chung, C. T. Y., S. B. Power, J. M. Arblaster, H. A. Rashid, and G. L. Roff (2014), Nonlinear precipitation response to El Niño and global warming in the Indo-Pacific, *Clim. Dyn.*, *42*(7–8), 1837–1856, doi:10.1007/s00382-013-1892-8.

Clarke, A. (1994), Why are surface equatorial ENSO winds anomalously westerly under anomalous large-scale convection?, *J. Clim.*, *7*, 1623–1627, doi:10.1175/1520-0442(1994)007<1623:WASEEW>2.0.CO;2.

Clarke, A. J. (2014), El Niño physics and El Niño predictability, *Annu. Rev. Mar. Sci.*, *6*, 79–99, doi:10.1146/annurev-marine-010213-135026.

Collins, M., et al. (2010), The impact of global warming on the tropical Pacific Ocean and El Niño, *Nat. Geosci.*, *3*(6), 391–397, doi:10.1038/ngeo868.

DiNezio, P. N., A. C. Clement, G. A. Vecchi, B. J. Soden, B. P. Kirtman, and S.-K. Lee (2009), Climate response of the equatorial Pacific to global warming, *J. Clim.*, *22*(18), 4873–4892, doi:10.1175/2009JCLI2982.1.

DiNezio, P. N., B. P. Kirtman, A. C. Clement, S.-K. Lee, G. A. Vecchi, and A. Wittenberg (2012), Mean climate controls on the simulated response of ENSO to increasing greenhouse gases, *J. Clim.*, *25*(21), 7399–7420, doi:10.1175/JCLI-D-11-00494.1.

Gill, A. E. (1980), Some simple solutions for heat-induced tropical circulation, *Q. J. R. Meteorol. Soc.*, *106*(449), 447–462, doi:10.1002/qj.49710644905.

Gill, A. E., and E. M. Rasmusson (1983), The 1982–83 climate anomaly in the equatorial Pacific, *Nature*, *306*, 229–234.

Jin, F., and S. An (1999), Thermocline and zonal advective feedbacks within the equatorial ocean recharge oscillator model for ENSO, *Geophys. Res. Lett.*, *26*(19), 2989–2992, doi:10.1029/1999GL002297.
Jin, F.-F., S. T. Kim, and L. Bejarano (2006), A coupled-stability index for ENSO, *Geophys. Res. Lett.*, *33*, L23708, doi:10.1029/2006GL027221.
Kim, S. T., W. Cai, F.-F. Jin, and J.-Y. Yu (2014a), ENSO stability in coupled climate models and its association with mean state, *Clim. Dyn.*, *42*(11–12), 3313–3321, doi:10.1007/s00382-013-1833-6.
Kim, S. T., W. Cai, F. Jin, A. Santoso, L. Wu, E. Guilyardi, and S. An (2014b), Response of El Niño sea surface temperature variability to greenhouse warming, *Nat. Clim. Change*, *4*, 786–790, doi:10.1038/NCLIMATE2326.
Linz, M., E. Tziperman, and D. MacMartin (2014), Process-based analysis of climate model ENSO simulations: Intermodel consistency and compensating errors, *J. Geophys. Res. Atmos.*, *119*, 7396–7409, doi:10.1002/2013JD021415.
Lübbecke, J. F., and M. J. McPhaden (2013), A comparative stability analysis of Atlantic and Pacific Niño modes, *J. Clim.*, *26*(16), 5965–5980, doi:10.1175/JCLI-D-12-00758.1.
Merryfield, W. J. (2006), Changes to ENSO under CO2 doubling in a multimodel ensemble, *J. Clim.*, *19*, 4009–4027.
Philip, S., and G. J. van Oldenborgh (2006), Shifts in ENSO coupling processes under global warming, *Geophys. Res. Lett.*, *33*, L11704, doi:10.1029/2006GL026196.
Power, S., F. Delage, C. Chung, G. Kociuba, and K. Keay (2013), Robust twenty-first-century projections of El Niño and related precipitation variability, *Nature*, *2*, doi:10.1038/nature12580.
Stevenson, S. L. (2012), Significant changes to ENSO strength and impacts in the twenty-first century: Results from CMIP5, *Geophys. Res. Lett.*, *39*, L17703, doi:10.1029/2012GL052759
Taylor, K. E., R. J. Stouffer, and G. A. Meehl (2012), An overview of CMIP5 and the experiment design, *Bull. Am. Meteorol. Soc.*, *93*(4), 485–498, doi:10.1175/BAMS-D-11-00094.1.
Trenberth, K. E., G. W. Branstator, D. Karoly, A. Kumar, N.-C. Lau, and C. Ropelewski (1998), Progress during TOGA in understanding and modeling global teleconnections associated with tropical sea surface temperatures, *J. Geophys. Res.*, *103*(C7), 14,291–14,324, doi:10.1029/97JC01444.
van Oldenborgh, G., S. Phillip, and M. Collins (2005), El Nino in a changing climate: A multi-model study El Nino, *Ocean Sci.*, *1*, 81–95, doi:10.5194/os-1-81-2005.
Vecchi, G. A., and B. J. Soden (2007), Global warming and the weakening of the tropical circulation, *J. Clim.*, *20*(17), 4316–4340, doi:10.1175/JCLI4258.1.
Yeh, S.-W., B. Dewitte, B. Y. Yim, and Y. Noh (2010), Role of the upper ocean structure in the response of ENSO-like SST variability to global warming, *Clim. Dyn.*, *35*(2–3), 355–369, doi:10.1007/s00382-010-0849-4.
Zebiak, S. E., and M. A. Cane (1987), A model El Nino-Southern Oscillation, *Mon. Weather Rev.*, *115*, 2262–2278.